ELSEVIER

Theoretical and Applied Fracture Mechanics 29 (1998) 213–217

theoretical and applied fracture mechanics

Analysis of material instability at an impact loaded crack tip

L. Chen, R.C. Batra *

Department of Engineering Science and Mechanics, Virginia Polytechnic Institute and State University, Blacksburg, VA 24061-0219, USA

Abstract

Assuming that a material point becomes unstable when the effective plastic strain there reaches a critical value, it is found that a material instability will initiate at a point on the crack-tip of an impulsively loaded prenotched plate that makes an angle of −14° to the notch-tip. This agrees well with the observed values of −5° to −15°.

1. Introduction

Experiments were performed [1,2] to study the deformation of a plate with two parallel cracks or notches and impacted by a cylindrical projectile of diameter equal to the spacing between the cracks. The crack tip deformation field is predominantly Mode II, i.e., in-plane shearing mode. The experimental results show that with an increase in the impact speed, the failure mode changes from a brittle crack along approximately 70°, to an adiabatic shear band along approximately −5° to −15° to the notch ligament. Similar experiments have been performed on a plate with a single edge crack [3,4]. It was found in [3] that a shear band propagates forward nearly parallel to the prenotch in a shear dominated zone and then arrests. Subsequently a different failure mode is initiated at a large positive angle to the notch ligament. Rough fracture surfaces and shear lips suggest that this growth is Mode I dominated. Failure mode transition has also been related to material properties [4]. Under similar conditions, different failure modes were observed in C-300 (a maraging) steel, but only shear banding mode of failure was observed in Ti-6Al-4V.

Using linear elastodynamics, Lee and Freund [5] analyzed the wave motion in a prenotched plate, showed that due to the effects of unloading waves, a transient, mixed-mode stress intensity factor field is induced near the crack tip, and determined time histories of stress intensity factors $K_{\mathrm{I}}(t)$ and $K_{\mathrm{II}}(t)$. The $K_{\mathrm{II}}(t)$ is large due to the incident compressive wave, but a time-dependent $K_{\mathrm{I}}(t)$ is also generated. Finite element simulations for this problem have also been made [6–8].

Assume that the plate material can be modeled as elastic/plastic, and Lee and Freund's [5] solution for the elastic problem holds outside of a circular region surrounding the notch-tip. By postulating that strains within the circular region vary as r^{-N} with $0 < N \leqslant 1$ and r the distance from the notch-tip, and that a material instability initiates in the direction of the maximum effective plastic strain, we ascertain the direction of the material instability. For the problem studied in [1,2], the material instability is found to initiate at an angle of −14° to the notch ligament which agrees well with the observed values of −5° to −15°.

* Corresponding author. Fax: +1 540 231 4574.

0167-8442/98/$19.00 © 1998 Elsevier Science Ltd. All rights reserved.
PII: S0167-8442(98)00032-9

2. Critical instability direction

The edge-cracked plate problem studied herein is shown schematically in Fig. 1. A rectangular Cartesian x, y-coordinate system is introduced in the plane of the plate with origin at the crack tip. Following the works in [6–8], assume that a plane strain mode of deformation prevails. The plate material is modeled as elastic-perfectly plastic, and the strain-displacement relations are assumed to be linear. In rectangular Cartesian coordinates, the effective plastic strain, γ_p, is given by

$$\gamma_p = \sqrt{\frac{2}{3} e^p_{ij} e^p_{ij}}, \tag{1}$$

where e^p_{ij} is the deviatoric plastic strain tensor, and a repeated index implies summation over the range of the index.

The impact load on the plate induces a combination of transient Mode I and II deformation fields near the crack tip [5]. For this mixed-mode field, the stress field in the elastic zone **E**, as determined by linear elastic dynamic fracture mechanics, is

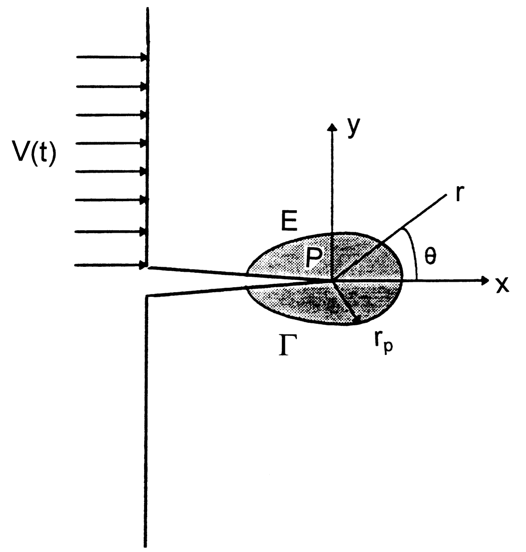

Fig. 1. Schematic of crack configuration and loading.

$$\begin{aligned}
\sigma_x &= \frac{K_I}{\sqrt{2\pi r}} \cos\frac{\theta}{2}\left(1 - \sin\frac{\theta}{2}\sin\frac{3\theta}{2}\right) \\
&\quad - \frac{K_{II}}{\sqrt{2\pi r}} \sin\frac{\theta}{2}\left(2 + \cos\frac{\theta}{2}\cos\frac{3\theta}{2}\right) \\
&= \frac{K_{II}}{\sqrt{2\pi r}}\left[\tan\left(\frac{\pi}{2}m^e\right)\cos\frac{\theta}{2}\left(1 - \sin\frac{\theta}{2}\sin\frac{3\theta}{2}\right)\right. \\
&\quad \left. - \sin\frac{\theta}{2}\left(2 + \cos\frac{\theta}{2}\cos\frac{3\theta}{2}\right)\right] \\
&\equiv \frac{K_{II}}{\sqrt{2\pi r}}\sigma_{x1}(m^e, \theta),
\end{aligned}$$

$$\begin{aligned}
\sigma_y &= \frac{K_I}{\sqrt{2\pi r}} \cos\frac{\theta}{2}\left(1 + \sin\frac{\theta}{2}\sin\frac{3\theta}{2}\right) \\
&\quad + \frac{K_{II}}{\sqrt{2\pi r}} \sin\frac{\theta}{2}\cos\frac{\theta}{2}\cos\frac{3\theta}{2} \\
&= \frac{K_{II}}{\sqrt{2\pi r}}\left[\tan\left(\frac{\pi}{2}m^e\right)\cos\frac{\theta}{2}\left(1 + \sin\frac{\theta}{2}\sin\frac{3\theta}{2}\right)\right. \\
&\quad \left. + \sin\frac{\theta}{2}\cos\frac{\theta}{2}\cos\frac{3\theta}{2}\right] \equiv \frac{K_{II}}{\sqrt{2\pi r}}\sigma_{y1}(m^e, \theta),
\end{aligned}$$

$$\begin{aligned}
\tau_{xy} &= \frac{K_I}{\sqrt{2\pi r}} \cos\frac{\theta}{2}\sin\frac{\theta}{2}\cos\frac{3\theta}{2} \\
&\quad + \frac{K_{II}}{\sqrt{2\pi r}} \cos\frac{\theta}{2}\left(1 - \sin\frac{\theta}{2}\sin\frac{3\theta}{2}\right) \\
&= \frac{K_{II}}{\sqrt{2\pi r}}\left[\tan\left(\frac{\pi}{2}m^e\right)\cos\frac{\theta}{2}\sin\frac{\theta}{2}\cos\frac{3\theta}{2}\right. \\
&\quad \left. + \cos\frac{\theta}{2}\left(1 - \sin\frac{\theta}{2}\sin\frac{3\theta}{2}\right)\right] \\
&\equiv \frac{K_{II}}{\sqrt{2\pi r}}\tau_{xy1}(m^e, \theta), \sigma_z = \nu(\sigma_x + \sigma_y),
\end{aligned} \tag{2}$$

where r is the distance from the crack tip, and θ the angle from the notch ligament, as shown in Fig. 1, ν is Poisson's ratio, and $m^e = (2/\pi)\tan^{-1}(K_I/K_{II})$ is the mode-mixity parameter introduced in [9]. The mixity parameter is useful in characterizing the near-tip field under mixed-mode conditions. The time dependence of the mixity parameter for this problem was studied in [5].

In terms of the von Mises yield criterion, the corresponding small-scale plastic zone radius, r_p, can be determined from Eq. (2), as

$$r_p = \frac{1}{\sigma_0^2}\frac{K_{\rm II}^2}{2\pi}\left\{\frac{1}{3}[(1-v+v^2)(\sigma_{x1}^2+\sigma_{y1}^2) -(1+2v-2v^2)\sigma_{x1}\sigma_{y1}] + \tau_{xy1}^2\right\} \equiv \frac{1}{\sigma_0^2}\frac{K_{\rm II}^2}{2\pi} r_{p1}(m^e,\theta), \tag{3}$$

where σ_0 is the yield stress in a quasistatic simple tension or compression test. The strain field at the boundary Γ, i.e. $r = r_p$, obtained by using Hooke's law and Eq. (2) is

$$\begin{aligned}
\varepsilon_x|_\Gamma &= \frac{1}{E}\frac{K_{\rm II}}{\sqrt{2\pi r_p}}[\sigma_{x1}(m^e,\theta)(1-v^2) - \sigma_{y1}(m^e,\theta)(v+v^2)] \\
&= \frac{\sigma_0}{E}\frac{1}{\sqrt{r_{p1}(m^e,\theta)}}[\sigma_{x1}(m^e,\theta)(1-v^2) - \sigma_{y1}(m^e,\theta)(v+v^2)] \equiv \frac{\sigma_0}{E}\varepsilon_{x\Gamma}(m^e,\theta); \\
\varepsilon_y|_\Gamma &= \frac{1}{E}\frac{K_{\rm II}}{\sqrt{2\pi r_p}}[\sigma_{y1}(m^e,\theta)(1-v^2) - \sigma_{x1}(m^e,\theta)(v+v^2)] \\
&= \frac{\sigma_0}{E}\frac{1}{\sqrt{r_{p1}(m^e,\theta)}}[\sigma_{y1}(m^e,\theta)(1-v^2) - \sigma_{x1}(m^e,\theta)(v+v^2)] \equiv \frac{\sigma_0}{E}\varepsilon_{y\Gamma}(m^e,\theta); \\
\gamma_{xy}|_\Gamma &= \frac{1+v}{E}\frac{K_{\rm II}}{\sqrt{2\pi r_p}}\tau_{xy1}(m^e,\theta) \\
&= \frac{(1+v)\sigma_0}{E}\frac{1}{\sqrt{r_{p1}(m^e,\theta)}}\tau_{xy1}(m^e,\theta) \\
&\equiv \frac{\sigma_0}{E}\gamma_{xy\Gamma}(m^e,\theta).
\end{aligned} \tag{4}$$

We assume that strains in zone **P** are proportional to r^{-N}, $1 \geqslant N > 0$. This was suggested in [9–11] for the strain distribution around a crack tip. For $r \ll 1$, the elastic strains can be neglected as compared to their plastic counterparts. Henceforth, consider points near the notch-tip with $r \ll 1$ and neglect elastic strains. Thus, at a point close to the notch-tip

$$\begin{aligned}
\varepsilon_x^p &= \left(\frac{r_p}{r}\right)^N \varepsilon_x\Big|_\Gamma = \left(\frac{K_{\rm II}^2}{2\sigma_0^2\pi}\right)^N \frac{\sigma_0}{E}\left(\frac{r_{p1}(m^e,\theta)}{r}\right)^N \varepsilon_{x\Gamma}(m^e,\theta) \equiv \left(\frac{K_{\rm II}^2}{2\sigma_0^2\pi r}\right)^N \frac{\sigma_0}{E}\varepsilon_{x1}^p(m^e,\theta), \\
\varepsilon_y^p &= \left(\frac{r_p}{r}\right)^N \varepsilon_y\Big|_\Gamma = \left(\frac{K_{\rm II}^2}{2\sigma_0^2\pi}\right)^N \frac{\sigma_0}{E}\left(\frac{r_{p1}(m^e,\theta)}{r}\right)^N \varepsilon_{y\Gamma}(m^e,\theta) \equiv \left(\frac{K_{\rm II}^2}{2\sigma_0^2\pi r}\right)^N \frac{\sigma_0}{E}\varepsilon_{y1}^p(m^e,\theta), \\
\gamma_{xy}^p &= \left(\frac{r_p}{r}\right)^N \gamma_{xy}\Big|_\Gamma = \left(\frac{K_{\rm II}^2}{2\sigma_0^2\pi}\right)^N \frac{\sigma_0}{E}\left(\frac{r_{p1}(m^e,\theta)}{r}\right)^N \gamma_{xy\Gamma}(m^e,\theta) \equiv \left(\frac{K_{\rm II}^2}{2\sigma_0^2\pi r}\right)^N \frac{\sigma_0}{E}\gamma_{xy1}^p(m^e,\theta).
\end{aligned} \tag{5}$$

Substitution from Eq. (5) into Eq. (1) yields

$$\gamma_p = \left(\frac{K_{\rm II}^2}{2\sigma_0^2\pi r}\right)^N \frac{\sigma_0}{E}\left\{\frac{2}{3}\Big[[\varepsilon_{x1}^p(m^e,\theta)]^2 + [\varepsilon_{y1}^p(m^e,\theta)]^2 + 2[\gamma_{xy1}^p(m^e,\theta)]^2\Big]\right\}^{1/2} \equiv \left(\frac{K_{\rm II}^2}{2\sigma_0^2\pi r}\right)^N \frac{\sigma_0}{E}\gamma_{p1}(m^e,\theta). \tag{6}$$

Thus the effective plastic strain depends on the mode-mixity parameter, m^e, and the angle θ. It was found in [5] that for the time interval of interest, the mode-mixity parameter nearly equals −0.25 when Poisson's ratio for plate's material is 0.25. Let m^e in Eq. (6) be a constant. Also, postulate that the instability occurs at the critical angle θ_i where the effective plastic strain γ_p reaches first the critical instability strain. Hence the critical angle θ_i is determined by

$$\frac{\partial \gamma_{p1}(m^e,\theta)}{\partial\theta} = 0, \qquad \frac{\partial^2\gamma_{p1}(m^e,\theta)}{\partial^2\theta} < 0. \tag{7}$$

This gives

$$\theta_i = \theta_i(m^e). \tag{8}$$

Numerical experiments with $N = 0.4$, 0.7 and 1.0 gave virtually identical curves between θ_i and m^e for $-0.5 \leqslant m^e \leqslant 0.5$. This is not surprising since the dependence of γ_{p1} upon m^e and θ is determined by the far-field elastic solution. Henceforth we set $N = 1.0$. The relationship between the critical instability angle, θ_i, and the mode mixity parameter, m^e, is shown in Fig. 2 for Poisson's ratios equal to 0.25 and 0.4. It is evident that an increase in Poisson's ratio increases the critical instability angle; however, the change is small. Also

$$\theta_i = 0 \quad \text{when } m^e = 0. \tag{9}$$

Thus under pure Mode II loading conditions, i.e., $K_I = 0$, the material instability occurs along the notch ligament. However, as mentioned above, a time-dependent Mode I stress intensity factor generally develops, i.e., $K_I \neq 0$, and the instability occurs at $\theta_i \neq 0$. For $m^e = -0.25$, $\theta_i = -14°$ which agrees well with the observed values of $-5°$ to $-15°$ [1].

Eq. (6) implies that γ_p is a function of K_I, K_{II} and θ since $m^e = (2/\pi)\tan^{-1}(K_I/K_{II})$. Numerical experiments with θ and K_{II} kept constant indicated that maximum values (infinity) of γ_p occur for $m_e = \pm 1$. However, when θ and K_I were kept fixed, γ_p assumed very large values for $|m^e| \leqslant 0.17$. Thus it is not transparent if the nonlinear equations

$$\frac{\partial \gamma_p}{\partial K_I} = 0, \qquad \frac{\partial \gamma_p}{\partial K_{II}} = 0, \qquad \frac{\partial \gamma_p}{\partial \theta} = 0 \tag{10}$$

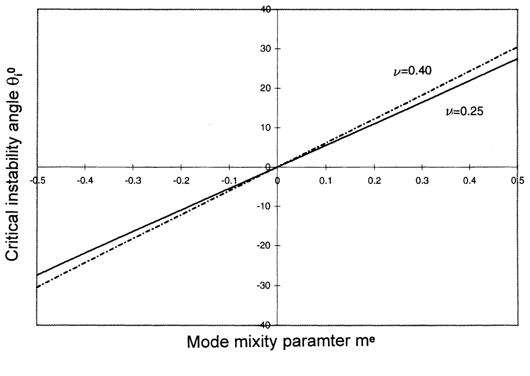

Fig. 2. Dependence of the critical instability angle on mode mixity parameter for $\nu = 0.25$ and 0.40.

have a unique solution K_I, K_{II} and θ, and that solution corresponds to a maximum value of γ_p.

3. Conclusions

It is found that the direction of material instability at the crack-tip in an impulsively loaded prenotched elastic-plastic plate is not sensitive to the exponent N of the singularity in strains near the crack-tip. The direction $-14°$ of material instability agrees well with the test values of $-5°$ to $-15°$.

Acknowledgements

This work was supported by the ONR grants N00014-94-1-1211 and N00014-98-1-0300 with Dr. Y.D.S. Rajapakse as the program manager.

References

[1] J.F. Kalthoff, Shadow optical methods of caustics, in: A.S. Kobayashi (Ed.), Handbook on Experimental Mechanics, Prentice-Hall, Englewood Cliffs, NJ, 1987, pp. 430–500.

[2] J.F. Kalthoff, S. Winkler, Failure mode transition at high strain rates of loading, in: C.Y. Chiem, H.D. Kunze, L.W. Meyer (Eds.), Proceedings of the International Conference on Impact Loading and Dynamic Behavior of Materials, Deutsche Gewsellschaft fur Metallkundcle, DGM, Bremen, 1988, pp. 185–196.

[3] J.J. Mason, A.J. Rosakis, G. Ravichandran, Full field measurements of the dynamic deformation field around a growing adiabatic shear band at the tip of a dynamically loaded crack or notch, J. Mech. Phys. Solids 42 (1994) 1679–1697.

[4] M. Zhou, A.J. Rosakis, G. Ravichandran, Dynamically propagating shear bands in impact-loaded prenotched plates – I. Experimental investigations of temperature signatures and propagation speed, J. Mech. Phys. Solids 44 (1996) 981–1006.

[5] Y.J. Lee, L.B. Freund, Fracture initiation due to asymmetric impact loading of an edge cracked plate, J. Appl. Mech. 57 (1990) 104–111.

[6] A. Needleman, V. Tvergaard, Analysis of a brittle-ductile transition under dynamic shear loading, Int. J. Fracture 32 (1995) 2571–2590.

[7] M. Zhou, G. Ravichandran, A.J. Rosakis, Dynamically propagating shear bands in impact-loaded prenotched plates – II. Numerical simulations, J. Mech. Phys. Solids 44 (1996) 1007–1032.

[8] R.C. Batra, N.V. Nechitailo, Analysis of failure modes in impulsively loaded prenotched steel plates, Int. J. Plasticity 13 (1997) 291–308.
[9] C.F. Shih, Small-scale yielding analysis of mixed plane strain crack problems, Fracture Analysis, ASTM STP 560 (1974) 187–210.
[10] J.R. Rice, G.F. Rosengren, Plane strain deformation near a crack tip in a power-law hardening material, J. Mech. Phys. Solids 16 (1968) 1–12.
[11] J.W. Hutchinson, Singular behavior at the end of a tensile crack in a hardening material, J. Mech. Phys. Solids 16 (1968) 13–31.